Catalytic Reaction Pathway for the Mitogen-Activated Protein Kinase ERK2

Claudine N. Prowse,[‡,§] Jonathan C. Hagopian,[§] Melanie H. Cobb,[∥] Natalie G. Ahn,[⊥] and John Lew*[,§]

Graduate Program in Biomedical Sciences, University of California, San Diego, California 92093, Department of Molecular, Cellular, & Developmental Biology, Interdepartmental Program in Biochemistry and Molecular Biology, University of California, Santa Barbara, California 93106, Department of Pharmacology, University of Texas Southwestern Medical Center, Dallas, Texas 75235, and Department of Chemistry & Biochemistry, Howard Hughes Medical Institute, University of Colorado, Boulder, Colorado 80303

Received February 4, 2000; Revised Manuscript Received March 21, 2000

ABSTRACT: The structural, functional, and regulatory properties of the *mitogen-activated protein kinases (MAP kinases)* have long attracted considerable attention owing to the critical role that these enzymes play in signal transduction. While several MAP kinase X-ray crystal structures currently exist, there is by comparison little mechanistic information available to correlate the structural data with the known biochemical properties of these molecules. We have employed steady-state kinetic and solvent viscosometric techniques to characterize the catalytic reaction pathway of the MAP kinase ERK2 with respect to the phosphorylation of a protein substrate, myelin basic protein (MBP), and a synthetic peptide substrate, ERKtide. A minor viscosity effect on k_{cat} with respect to the phosphorylation of MBP was observed ($k_{cat} = 10 \pm 2\ s^{-1}$, $k_{cat}^{\eta} = 0.18 \pm 0.05$), indicating that substrate processing occurs via slow phosphoryl group transfer ($12 \pm 4\ s^{-1}$) followed by the faster release of products ($56 \pm 4\ s^{-1}$). At an MBP concentration extrapolated to infinity, no significant viscosity effect on $k_{cat}/K_{m(ATP)}$ was observed ($k_{cat}/K_{m(ATP)} = 0.2 \pm 0.1\ \mu M^{-1}\ s^{-1}$, $k_{cat}/K_{m(ATP)}^{\eta} = -0.08 \pm 0.04$), consistent with rapid-equilibrium binding of the nucleotide. In contrast, at saturating ATP, a full viscosity effect on k_{cat}/K_m for MBP was apparent ($k_{cat}/K_{m(MBP)} = 2.4 \pm 1\ \mu M^{-1}\ s^{-1}$, $k_{cat}/K_{m(MBP)}^{\eta} = 1.0 \pm 0.1$), while no viscosity effect was observed on k_{cat}/K_m for the phosphorylation of ERKtide ($k_{cat}/K_{m(ERKtide)} = (4 \pm 2) \times 10^{-3}\ \mu M^{-1}\ s^{-1}$, $k_{cat}/K_{m(ERKtide)}^{\eta} = -0.02 \pm 0.02$). This is consistent with the diffusion-limited binding of MBP, in contrast to the rapid-equilibrium binding of ERKtide, to form the ternary Michaelis complex. Calculated values for binding constants show that the estimated value for $K_{d(MBP)}$ ($\leq 0.5\ \mu M$) is significantly lower than that of the measured $K_{m(MBP)}$ ($4.2 \pm 0.8\ \mu M$). Furthermore, MBP binds to the ERK2·ATP complex at least 1500-fold more tightly than does ERKtide ($K_{d(ERKtide)} \geq 1.5$ mM). The dramatically higher catalytic efficiency of MBP in comparison to that of ERKtide (~600-fold difference) is largely attributable to the slow dissociation rate of MBP ($\leq 1.2\ s^{-1}$) versus that of the synthetic peptide ($\geq 56\ s^{-1}$), from the ERK2 active site.

It is presently recognized that growth factor signaling in mammalian cells is mediated by a network of signal transduction pathways which are both complex and diverse. All mitogens, however, share one commonality in their mechanisms of action: they elicit the downstream response of a *mitogen-activated protein kinase*. This family of enzymes, the MAP[1] kinases, comprises the ERK,[1] JNK,[1] and p38 protein kinase subfamilies. All participate in signal transduction as members of a three-tier protein phosphorylation cascade in which the MAP kinases are regulated by a MAP kinase kinase (MKK) which, in turn, is under the upstream control of a MAP kinase kinase kinase (MKKK). While the JNKs and p38 kinase families are activated primarily in response to cellular stresses, the ERKs are activated in response to peptide growth factors and phorbol esters. The MAP kinases catalyze the phosphorylation of a number of cellular protein targets which include transcription factors and other protein kinases, ultimately resulting in the pleiotropic effects associated with mitogen signaling (for review, see refs *1*−*3*).

Among members of the protein kinase superfamily, the MAP kinases display unique biochemical properties in terms of both their mechanism of regulation and also their substrate specificity. While the activation of most, but not all, protein kinases requires the phosphorylation of a single site within a structurally conserved segment termed the "activation loop" (*4*), the MAP kinases are activated by dual-phosphorylation on a conserved threonine phosphorylation site and an additional neighboring tyrosine residue (-X-T-X-Y-X-) (*2*). The phosphorylation of both residues is essential for full catalytic activity (*5*) and is mediated by a dual-specificity MAP kinase kinase (*6*). In addition, the substrate amino acid sequence specificity of MAP kinases includes the stringent recognition of a proline residue immediately carboxyl-terminal to the site of phosphorylation within the target substrate (-X-P-X-S/T-P-X-) (*7, 8*). This property is shared only with the cyclin-dependent kinases which, although they display a distinct substrate recognition motif (*9*), together define a family of enzymes with novel target substrate specificity referred to as the *proline-directed protein kinases.*

* Correspondence should be addressed to this author. Tel: (805) 893-5336, fax: (805) 893-4724, email: lew@lifesci.ucsb.edu.
‡ University of California, San Diego.
§ University of California, Santa Barbara.
∥ University of Texas Southwestern Medical Center.
⊥ University of Colorado.

[1] Abbreviations: MBP, myelin basic protein; ERK, extracellular-regulated kinase; JNK, jun N-terminal kinase; MAP, mitogen-activated protein; cAPK, 3′,5′-cyclic AMP-dependent protein kinase.

10.1021/bi000277b CCC: $19.00
Published on Web 04/26/2000

In an effort to understand the structural and mechanistic basis for their physiological regulation and function, the high-resolution X-ray crystallographic structures of several MAP kinases have recently been solved. These include structures of the wild-type dual-phosphorylated (*10*) and unphosphorylated rat ERK2 species (*11*), as well as four ERK2 phosphorylation site mutants (*12*), and a mutant in which the invariant active site lysine (residue 52) has been substituted with arginine (*13*). While X-ray diffraction has thus provided a large database of structural information regarding the role of phosphorylation in the activation process of ERK2, there is currently little mechanistic information available to ultimately correlate the structural data with the known biochemical properties of this molecule. Furthermore, the three-dimensional structure of a MAP kinase cocrystallized with a substrate, or substrate analogue, has not been solved. Thus, little structural and mechanistic information addressing the substrate recognition properties of this enzyme family is available.

In this study, we report the catalytic parameters for substrate binding, phosphoryl group transfer, and product release for the phosphorylation of a protein substrate, MBP,[1] by ERK2. In addition, we compare the catalytic efficiency of MBP to a synthetic peptide substrate, ERKtide. Our studies provide a kinetic framework by which the role of dual-phosphorylation in catalytic activation and the substrate recognition properties of ERK2 may be understood on a detailed structure/mechanistic level.

MATERIALS AND METHODS

Reagents were obtained from the following commercial sources. Potassium chloride (KCl), ethylenediaminetetraacetic acid (EDTA), magnesium chloride ($MgCl_2$), 3-(*N*-morpholino)propanesulfonic acid (MOPS), sucrose, dithiothreitol (DTT), and urea (ACS grade) were purchased from Fisher. Adenosine 5′-triphosphate (ATP), phosphoenol pyruvate (PEP), nicotinamide adenine dinucleotide, reduced (NADH), pyruvate kinase (PK), lactate dehydrogenase (LDH), Ficoll-400, brain acetone powder, and 18 kDa bovine MBP were purchased from Sigma. [γ-^{32}P]ATP was purchased from ICN.

Peptide Synthesis. "ERKtide" (ATGPLSPGPFGRR) was synthesized by FMOC solid-phase synthesis and purified by reversed-phase HPLC on a DeltaPak C-18 column with an acetonitrile/water (0.05% trifluoroacetic acid) gradient by the AIC Peptide Synthesis Facility, Department of MCD Biology, UCSB. Analysis by electrospray mass spectrometry was carried out at the Department of Chemistry Mass Spectrometry Facility, UCSB.

MBP Purification. The bovine brain 18 kDa isoform of myelin basic protein (MBP) was isolated from brain acetone powder (Sigma B0508) based on a published protocol (*14*) which we have modified. Briefly, 25 g of brain acetone powder was dissolved in 450 mL of 0.03 N HCl, 1 μM pepstatin A, pH 3.0, for 2 h at 4 °C. The extract was centrifuged at 12 500 rpm in a Sorvall GSA rotor for 30 min at 4 °C. The pellet was re-extracted, and the supernatants were pooled. All subsequent manipulations were carried out at room temperature. Urea was dissolved into the pooled supernatants to a final concentration of 4 M, and the solution was adjusted to 10 mM citrate, pH 5.0. The sample (~700 mL) was loaded at a rate of 4−5 mL/min onto an SP-Sepharose column (4 × 2.5 cm) that had been preequilibrated with 10 mM citrate, 4 M urea, pH 5.0. After sample loading, the column was washed with 50 mL of 20 mM glycine, 50 mM NaCl, 4 M urea, pH 9.5, or until no further protein eluted as measured by Bradford assay. Bound protein was eluted at 1 mL/min in steps with buffer containing 20 mM glycine, 4 M urea, pH 9.5, and 50, 100, 200, or 300 mM NaCl. The eluate was collected in 5 mL fractions and protein monitored by Bradford assay. Under these conditions, the majority and most highly pure fractions of MBP eluted at 200 mM NaCl. The MBP-containing fractions were dialyzed 10 000-fold against water, and lyophilized. Protein concentration determination was based on an extinction coefficient calculated from the amino acid composition (*15*) of bovine MBP[2] (ϵ_{280} = 10 800 cm^{-1} M^{-1}). Typically, approximately 200 mg of highly purified MBP was obtained from 25 g of brain acetone powder.

MEK1 Expression and Purification. Recombinant human MEK1 was expressed in *E. coli* as a constitutively active mutant (G7B: N4/S218D/M219D/N221D/S221D) that is N-terminally-fused to GST. Briefly, the cDNA for the constitutively active MEK1 in pRSETa (*16*) was subcloned into a pGEX-KG expression vector. The GST-MEK1 construct was transformed into *E. coli* strain BL21-DE3 and grown at 37 °C to A_{600} = 0.8 from a frozen glycerol stock, and protein expression was induced by addition of 0.4 mM isopropyl β-D-galactopyranoside for 4 h at 30 °C. The bacteria were harvested by centrifugation at 5000 rpm × 15 min (Beckman JA9 rotor); the cell pellet from 1 L of culture was resuspended in 20 mL of 30 mM MOPS, pH 7.4, 1 mM EDTA, 1 mM DTT, 50 mM NaCl, 10% glycerol, and 0.25% Tween-20. Protease inhibitors (0.5 mM PMSF, 1 mM benzamidine, 1 μg/mL pepstatin, 1 μg/mL leupeptin, 1 μg/mL aprotinin) were added and the bacteria lysed by sonication (5 × 20 s bursts in ice). The lysate was cleared at 15 000 rpm for 30 min in a Sorvall SS34 rotor, and the supernatant was mixed with 1.5 mL of glutathione−agarose resin (Sigma) and incubated end-over-end for 1 h, 4 °C. The resin was washed once with 30 mM MOPS, pH 7.4, 0.1 mM EDTA, 50 mM NaCl, 10% glycerol, 0.25% Tween-20, 1 mM DTT, and then a second time without glycerol and Tween-20. Protein was eluted in the same buffer containing 10 mM reduced glutathione (GSH), and fractions containing protein were stored in 10% glycerol at −70 °C. From 1 L of bacterial culture, 1 mg of total protein is typically obtained, of which a minor fraction (<10%) represents GST-MEK1.

ERK2 Expression, Purification, and Activation. The cDNA encoding rat ERK2 N-terminally-fused to a hexa-histidine tag was expressed in *E. coli* and purified as described previously (*17*). The in vitro activation of ERK2 was carried out by incubation of 1 mg (total protein) of GST-MEK1 with 2 mg of Ni^{2+}-NTA-purified ERK2 in the presence of 5 mM ATP, 20 mM $MgCl_2$, 20 mM MOPS, 4 mM DTT, pH 7.4, and activation was allowed to proceed at room temperature for 60 min, at which time activation was near 100% complete. The reaction mixture was chromatographed over Uno Q anion exchange chromatography (BioRad BioLogics System) and washed, and the bound proteins were eluted in a 50−300 mM NaCl gradient. The activated ERK2 elutes as a single peak at 120 mM NaCl and is nearly homogeneous

[2] Swissprot accession no. P02687.

as judged by 12% SDS−PAGE. The stoichiometry of phosphorylation was confirmed to be 2 mol of PO_4/mol of ERK2 by electrospray mass spectrometry. ERK2 protein concentration for all experiments was determined from an extinction coefficient calculated from its primary amino acid sequence (*15*) ($\epsilon_{280} = 44\ 825\ cm^{-1}\ M^{-1}$). The enzyme was stable for at least 2 h at room temperature, 1 week at 0 °C, and several months at −80 °C.

Kinetic Assays and Data Analysis. The phosphorylation of MBP by ERK2 was monitored using a coupled spectrophotometric assay (*18*). The concentrations of the coupling reagents were as follows: 15 units/mL LDH, 7.5 units/mL PK, 1 mM PEP, and 130 μM NADH. All reactions were performed in phosphorylation buffer (20 mM MOPS, pH 7.4, 50 mM KCl, 0.1 mM EDTA, 1 mM DTT, 10 mM $MgCl_{2(total)}$) with coupling reagents in a total volume of 75 μL at 23 °C. Typically, reactions containing ERK2 and ATP were initiated by the addition of MBP. Progress of the reaction was monitored continuously by a decrease in absorbance at 340 nm in a Shimadzu UV1601 spectrophotometer. Initial velocities were obtained from the linear portion of the progress curve, and calculated based on an extinction coefficient for NADH of 6220 $cm^{-1}\ M^{-1}$at 340 nm. Assays were corrected for ATPase activity, taken as the observed rate in the absence of MBP.

Steady-state kinetic parameters were determined by nonlinear least-squares analysis of initial velocity data obtained from 6−8 different concentrations of MBP at 6 different fixed concentrations of ATP. The data were globally fit to the following equation for a two-substrate reaction using the program Scientist (Micromath Inc., UT):

$$v = VAB/(K_{iA}K_{mB} + K_{mB}A + K_{mA}B + AB)$$

where v is the initial velocity, V is the maximal initial velocity, A and B are the fixed and varied substrate concentrations, respectively, K_m is the Michaelis constant, and K_{iA} is the dissociation constant for A. k_{cat} was determined by dividing the maximal initial velocity by the enzyme concentration.

The full progress curve for the phosphorylation of MBP was carried out under the conditions described above with exception to the concentrations of coupling agents, which were 30 units/mL LDH, 15 units/mL PK, and 2 mM PEP. Data were imported into Scientist and fit to a numerically integrated form of the following model file by nonlinear least-squares regression analysis:

$$dS/dt = -k_{cat}ES/[S + K_m(1 + P/K_p)]$$

where E is the concentration of enzyme, S is the concentration of MBP, P is the concentration of phospho-MBP, and K_p is the product inhibitory constant. k_{cat} and K_m are as described above, and were fixed at the values obtained from initial velocity studies. K_p and S_0 (S at $t = 0$) were allowed to float.

ERKtide phosphorylation was monitored by a radioisotope assay in which the direct incorporation of ^{32}P from [γ-^{32}P]-ATP into the peptide substrate was measured. Reactions were carried out in phosphorylation buffer containing ERK2 and varied amounts of one substrate with the other held fixed. Reactions were initiated by the addition of 1 mM [γ-^{32}P]-ATP (200 cpm/pmol) and allowed to proceed at 23 °C for 10 min, at which time the reaction was terminated with 25% acetic acid. Reaction samples were spotted onto a 20 cm × 20 cm square sheet of phosphocellulose paper (Whatman P81) 2.5 cm from the bottom, and subjected to ascending paper chromatography in 20 mM H_3PO_4, pH 2 (1.2 mL of 85% H_3PO_4/L of H_2O). In this system, ATP migrates with the solvent front and is resolved from the phosphorylated peptide product which remains at the origin. Papers were dried, and radioactivity corresponding to the phosphopeptide spots was excised and quantified by Cerenkov counting.

Solvent Viscosometric Studies. Steady-state assays were carried out as described above in buffer containing varied sucrose or Ficoll 400. Relative solvent viscosity (η^{rel}) was determined from the equation:

$$\eta^{rel} = (t/t^o)(\rho/\rho^o)$$

where η^{rel} is the solvent viscosity relative to buffer containing no viscosogen, t is the solvent transit time measured by an Ostwald capillary viscometer, and ρ is the solvent specific gravity (*19*). Superscript 'o' indicates buffer with no viscosogen.

RESULTS

Steady-State Kinetic Parameters for the Phosphorylation of MBP. The conventional substrate used to assay MAP kinase activity has traditionally been myelin basic protein (MBP). The phosphorylation of MBP (169 amino acids) by ERK2 has been mapped to a single site (Thr^{97}) (*20*), and we and others have shown that this substrate is among the most highly efficient ($k_{cat}/K_m = 2.4 \pm 1\ \mu M^{-1}\ s^{-1}$) of those identified for ERK2 (*13*, *21*). As a source of this substrate for our studies, we have purified MBP from a bovine brain acetone powder following a simple procedure which yields large quantities of the highly purified protein.

To characterize the steady-state kinetic properties of ERK2, we first carried out a time course of MBP phosphorylation to establish initial velocity conditions using a coupled spectrophotometric assay. At saturating concentrations of ATP, the time-dependent reaction profile deviated from linearity early in the reaction time course. The kinetics of the full time course could be fit to a Michaelis−Menten model describing competitive product inhibition ($K_p \approx 0.5\ \mu M$) (Figure 1). All initial velocity studies were carried out using a continuous assay in which the linearity of the initial portion of the reaction profile was carefully monitored. When initial conditions were met, the dependence of the initial rate on the concentration of one substrate with the other held fixed obeyed simple Michaelis−Menten kinetics. Furthermore, we have found that the steady-state kinetic behavior of our purified MBP is identical to MBP obtained commercially,[3] the traditional source of this substrate (data not shown).

A data set of initial velocities was obtained by varying the concentration of MBP at several fixed concentrations of ATP (Figure 2) which was analyzed by global fitting procedures using nonlinear regression analysis (see Materials and Methods). Unlike conventional fitting methods in which data corresponding to each fixed concentration of ATP are

[3] Sigma (M1891).

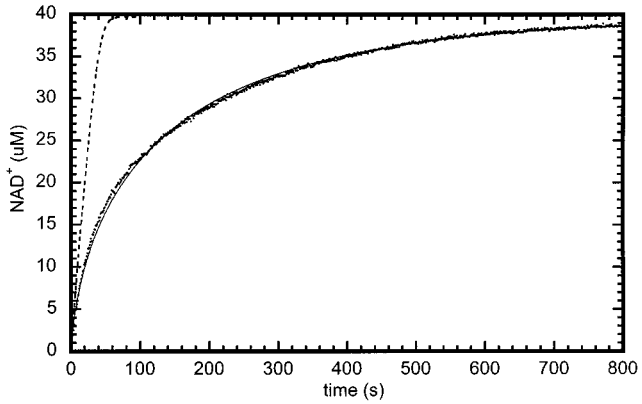

FIGURE 1: Reaction time course for the phosphorylation of MBP. The time-dependent phosphorylation of MBP was monitored by the decrease in absorbance at 340 nm using a coupled spectrophotometric assay, as described under Materials and Methods. Absorbance units (A_{340}) were converted to μM NAD^+ by the following equation: $\mu M\ NAD^+ = -(a_0 - a_t)/\epsilon_{340(NADH)}$, where a_0 and a_t are the absorbance values at time 0 and time t, respectively, and $\epsilon_{340(NADH)}$ is the extinction coefficient for NADH at 340 nM (0.00623 $cm^{-1}\ \mu M^{-1}$). The data were modeled to the equation: $dP/dt = k_{cat}ES/[S + K_m(1 + P/K_p)]$ by numerical integration using the program Scientist (Micromath Software). k_{cat} and K_m were set at 10 s^{-1} and 4 μM, respectively, which were obtained from initial velocity studies (see Table 1), while K_p was allowed to float. The best-fit curve was obtained by nonlinear regression analysis and is superimposed on the data. The dashed line is the curve simulated in the absence of product inhibition (K_p was fixed at 1000 μM). The concentration of ERK2 was 0.12 μM; the initial concentration of MBP was 20 μM; ATP was fixed at 1 mM.

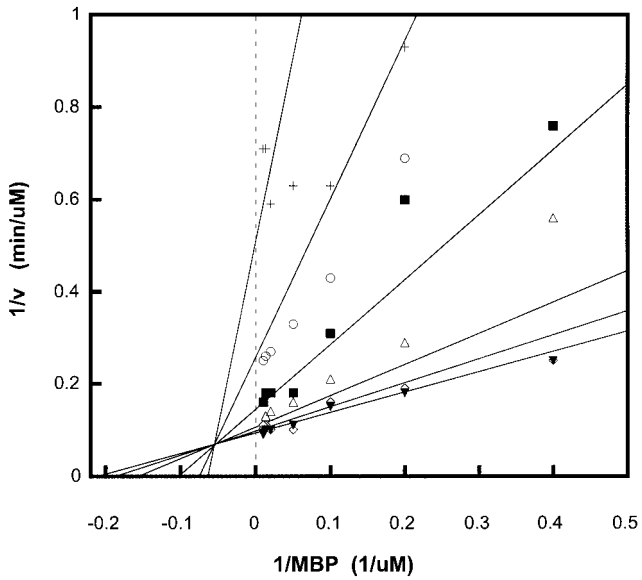

FIGURE 2: Steady-state kinetic analysis of MBP phosphorylation. Initial velocities were determined using a coupled spectrophotometric assay, and steady-state kinetic parameters were obtained by nonlinear regression analysis of the raw, untransformed data. Data were globally fit to a model describing two-substrate sequential binding (see Materials and Methods). Both the experimental data and the calculated regression curves are shown in the form of a double-reciprocal plot. The concentration of ERK2 was 30 nM. ATP concentrations were fixed at 10, 25, 75, 250, 500, and 1000 μM (from top to bottom).

fit individually, the kinetic parameters obtained by global analysis are constrained by the entire matrix of ATP versus MBP concentrations, simultaneously. As a consequence, the final fit of any individual curve may appear poor in comparison to conventional fitting methods but, in fact, represents the best possible fit to the model. Rather, the goodness of fit is more accurately reflected in the error associated with each parameter, which in this case is 20% or less. The steady-state kinetic parameters for the phosphorylation of MBP by ERK2 are shown in Table 1. The measured values for k_{cat}, $K_{m(MBP)}$, and $K_{m(ATP)}$ correspond to those that have been reported previously for the His_6-tagged (*13*) as well as the untagged (*20*, *21*) enzyme, thus demonstrating that the hexahistidine tag does not affect the kinetic behavior of ERK2.

Table 1: Kinetic and Thermodynamic Constants for Phosphorylation of MBP

parameter	value	method of determination
k_{cat}	$10 \pm 2\ s^{-1}$	measured
$k_{cat}/K_{m(MBP)}$	$2.4 \pm 1\ \mu M^{-1}\ s^{-1}$	$k_{cat}/K_{m(MBP)}$
$k_{cat}/K_{m(ATP)}$	$0.2 \pm 0.1\ \mu M^{-1}\ s^{-1}$	$k_{cat}/K_{m(ATP)}$
k_{cat}^{η}	0.18 ± 0.05	measured
$k_{cat}/K_{m(MBP)}^{\eta}$	1.0 ± 0.1	measured
$k_{cat}/K_{m(ATP)}^{\eta}$	-0.08 ± 0.04	measured
$k_{2(MBP)}$	$2.4 \pm 1\ \mu M^{-1}\ s^{-1}$	$(k_{cat}/K_{m(MBP)})/(k_{cat}/K_{m(MBP)}^{\eta})$
$k_{-2(MBP)}$	$\leq 1.2\ s^{-1}$	$k_3(1 - k_{cat}/K_{m(MBP)}^{\eta})/(k_{cat}/K_{m(MBP)}^{\eta})$
$k_{2(ATP)}$	$\geq 2\ \mu M^{-1}\ s^{-1}$	$(k_{cat}/K_{m(ATP)})/(k_{cat}/K_{m(ATP)}^{\eta})$
$k_{-2(ATP)}$	$\geq 120\ s^{-1}$	$k_3(1 - k_{cat}/K_{m(ATP)}\eta)/(k_{cat}/K_{m(ATP)}^{\eta})$
k_3	$12 \pm 4\ s^{-1}$	$k_{cat}/(1 - k_{cat}^{\eta})$
k_4	$56 \pm 4\ s^{-1}$	k_{cat}/k_{cat}^{η}
$K_{m(MBP)}$	$4.2 \pm 0.8\ \mu M$	measured
$K_{m(ATP)}$	$47 \pm 8\ \mu M$	measured
$K_{i(ATP)}$	$210 \pm 85\ \mu M$	measured
$K_{d(MBP)}$	$\leq 0.5\ \mu M$	$k_{-2(MBP)}/k_{2(MBP)}$
$K_{d(ATP)}$	$57 \pm 20\ \mu M$	$K_m/[k_4/(k_3 + k_4)]$

Scheme 1

$$E^A + B \underset{k_{-2}}{\overset{k_2}{\rightleftharpoons}} E^AB \xrightarrow{k_3} E^PQ \xrightarrow{k_4} E + P + Q$$

Solvent Viscosometric Studies: (A) Fixed ATP, Varied MBP. The diffusion constant for a small molecule in solution is inversely proportional to the relative microviscosity of the bulk solvent (*22*). Consequently, solvent viscosity studies have been classically used to isolate those processes within an enzymatic reaction pathway which are subject to diffusion-control (*23*, *24*). This technique has been used to demonstrate that product release is cleanly rate-determining with respect to the overall rate of substrate processing (k_{cat}) in cAMP-dependent protein kinase (*25*), and partially rate-determining in both the C-terminal src kinase *csk* (*26*) and the oncoprotein *v-fps* (*27*).

We have partitioned the diffusion-controlled steps within the catalytic reaction pathway of ERK2 by examining the steady-state phosphorylation of MBP in the presence of sucrose. The data were analyzed according to the reaction pathway shown as Scheme 1, where E is the enzyme and A and B are the fixed and varied substrates, respectively. Under saturating conditions of A:

$$k_{cat} = k_3k_4/(k_3 + k_4) \quad (1)$$

$$k_{cat}/K_{m(B)} = k_2k_3/(k_{-2} + k_3) \quad (2)$$

While k_{cat} is a measure of the rate of substrate turnover, k_{cat}/K_m is a measure of the rate of substrate capture to form a complex competent to produce product.

In the presence of a microviscosogen, the rate constants which dictate the diffusion-controlled steps in k_{cat} (k_4) or k_{cat}/K_m (k_2, k_{-2}) will be decreased by a factor of $1/\eta^{rel}$, where

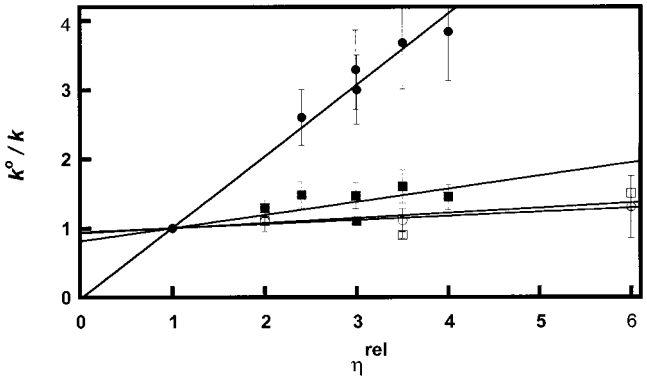

FIGURE 3: Solvent viscosity effects on k_{cat} and $k_{cat}/K_{m(MBP)}$ for the phosphorylation of MBP. Viscosity effects on k_{cat} or $k_{cat}/K_{m(MBP)}$ were determined as a function of increasing concentrations of sucrose or Ficoll 400. k^o/k corresponds to $k_{cat}{}^o/k_{cat}$ or $(k_{cat}/K_m)^o/(k_{cat}/K_m)$. The superscript 'o' denotes the absence of viscosogen. η^{rel} is the relative solvent viscosity as defined under Materials and Methods. ATP was fixed at 1 mM; MBP was varied. (●) $(k_{cat}/K_{m(MBP)})^o/(k_{cat}/K_{m(MBP)})$ in the presence of sucrose; (■) $k_{cat}{}^o/k_{cat}$ in the presence of sucrose; (○) $(k_{cat}/K_{m(MBP)})^o/(k_{cat}/K_{m(MBP)})$ in the presence of Ficoll 400; (□) $k_{cat}{}^o/k_{cat}$ in the presence of Ficoll 400.

η^{rel} is the solvent viscosity relative to buffer containing no viscosogen (*22*). By comparison, the rate of chemistry occurring within the active site is predicted to be unaffected by viscosometric perturbation of the solvent. The magnitude of decrease in either k_{cat} or k_{cat}/K_m plotted as a function of the relative solvent viscosity is a linear relationship, having slope values of $k_{cat}{}^{\eta}$ and $k_{cat}/K_{m(B)}{}^{\eta}$, respectively (*28*, *29*), where

$$k_{cat}{}^{\eta} = k_3/(k_3 + k_4) \quad (3)$$

$$k_{cat}/K_{m(B)}{}^{\eta} = k_3/(k_{-2} + k_3) \quad (4)$$

Both $k_{cat}{}^{\eta}$ and $k_{cat}/K_{m(B)}{}^{\eta}$ can vary between the theoretical limits of 0 [if chemistry (k_3) is cleanly rate-determining] and 1 [if diffusion-controlled steps (k_4, k_2, k_{-2}) are rate-determining]. Thus, solvent viscosity effects allow the absolute rate constant, or lower limit thereof, for each step in a simple three-step catalytic mechanism, to be inferred.

The effect of increasing solvent viscosity on the steady-state kinetic parameters for the phosphorylation of MBP by ERK2 is shown in Figure 3. At saturating ATP (1 mM), a small viscosity effect at high MBP concentrations was observed ($k_{cat}{}^{\eta} = 0.2 \pm 0.05$), placing estimates for the rates of phosphoryl group transfer and product release at 12 ± 4 and 56 ± 4 s^{-1}, respectively. By comparison, a full viscosity effect was observed on $k_{cat}/K_{m(MBP)}$ ($k_{cat}/K_{m(MBP)}{}^{\eta} = 1.0 \pm 0.1$), which predicts that the dissociation rate constant for MBP can be no greater than 1.2 s^{-1}. The kinetic constants measured directly or derived from the viscosity data are summarized in Table 1.

When high concentrations of cosolvent are introduced into a reaction medium, there is the inherent concern that observed altered reaction rates may be ascribed to altered protein stability, erroneously brought about by changes in osmotic pressure, dielectric constant, or other macroviscosogenic properties of the cosolvent, rather than to altered diffusional properties resulting specifically from a change in the solvent microviscosity. To test this, we examined the kinetics of MBP phosphorylation in the presence of a

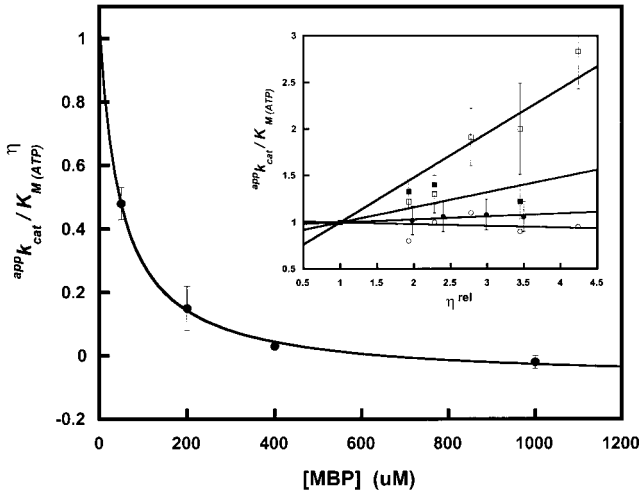

FIGURE 4: Solvent viscosity effects on $k_{cat}/K_{m(ATP)}$. ATP was either varied or fixed at 20 μM at various fixed concentrations of MBP, and solvent viscosity effects on $^{app}k_{cat}/K_{m(ATP)}$ were determined. Values for $^{app}k_{cat}/K_{m(ATP)}{}^{\eta}$ at fixed values of [MBP] were fit to the following equation: $y = -ax/(b + x) + c$, where a is the total change in the viscosity effect, b is the [MBP] at $0.5a$, and c is the y-intercept value. The data from which the viscosity effects (slope values) were derived are shown in the inset [50 μM (□), 200 μM (■), 400 μM (●), and 1 mM (○) MBP]. The viscosogenic agent was sucrose. The concentration of ERK2 was 20 nM.

macroviscosogen, Ficoll 400. Such high molecular weight polymers are expected to result in altered macrovicosogenic properties of the solvent without affecting the diffusional rates of small molecules in solution (*30*). We observed no viscosity effect on either k_{cat} or $k_{cat}/K_{m(MBP)}$ when Ficoll 400 was the viscosogenic agent (Figure 3). This is proof that the viscosity effects observed using sucrose are due to altered diffusional rates, and are not attributable to changes in the macroviscosogenic properties of this cosolvent. To test if sucrose itself might specifically perturb the enzyme structure, we examined the effects of increased sucrose concentration on the rate of ATPase activity under high (1 mM) ATP concentrations. No viscosity effect was observed on k_{cat} (not shown), suggesting that the ERK2 active site is structurally unaffected by high sucrose concentrations. When the ATP concentration was doubled at the highest relative viscosity, the rate of MBP phosphorylation did not change, confirming that under these conditions initial velocity measurements represent true k_{cat} values.

(B) Fixed MBP, Varied ATP. We tested the effects of increased solvent viscosity on the catalytic reaction mechanism when the concentration of ATP was varied and MBP was fixed. At saturating MBP (200 μM), the viscosity effect on k_{cat} was identical within error ($k_{cat}{}^{\eta} = 0.18 \pm 0.05$) to that observed when MBP was varied under saturating ATP. When the viscosity effect on the apparent $k_{cat}/K_{m(ATP)}$ was examined, it was found that $^{app}k_{cat}/K_{m(ATP)}{}^{\eta}$ varied inversely as a function of the fixed concentration of MBP (Figure 4, inset). The relationship between $^{app}k_{cat}/K_{m(ATP)}{}^{\eta}$ and MBP concentration fit well to a hyperbolic equation with extrapolated values of $^{app}k_{cat}/K_{m(ATP)}{}^{\eta}$ equal to 1.0 ± 0.2 and -0.08 ± 0.04, at zero and infinite MBP, respectively (Figure 4). The observed visocosity effect on $^{app}k_{cat}/K_{m(ATP)}$ as a function of MBP concentration allows the kinetic mechanism of substrate addition to be deduced. For example, our steady-state data (Figure 2) together with data from ATPase experiments (not shown) along with published crystal-

Scheme 2

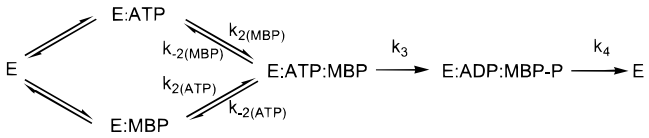

lographic information suggest a mechanism that is either random or ordered with ATP binding first (see Discussion). The ordered mechanism, however, would predict an increasing, as opposed to decreasing, viscosity effect on $^{app}k_{cat}/K_{m(ATP)}$ as the MBP concentration is increased (see Discussion). Such a prediction is contrary to our observations (Figure 4), which show a clear decreasing value for $^{app}k_{cat}/K_{m(ATP)}^{\eta}$ as a function of MBP concentration. Therefore, taken together, our data are consistent with the random addition of ATP and MBP to the ERK2 active site. The kinetic constants derived for the overall phosphorylation of MBP (Scheme 2) are summarized in Table 1.

(C) Phosphorylation of ERKtide. Small synthetic peptides serve as efficient substrates for a number of protein kinases (*31*, *32*). A synthetic peptide, ERKtide, has been identified as the optimal substrate sequence for ERK1 and ERK2 from a random peptide combinatorial library screen (*33*). While this is true, the catalytic efficiency of ERKtide ($k_{cat}/K_{m(ERKtide)}$) is more than 2 orders of magnitude lower than that of MBP (*13*). To determine the source of the large difference in catalytic efficiency between MBP and ERKtide, we carried out a viscosometric study on the phosphorylation of ERKtide. In steady-state kinetic assays, the saturation of ERK2 with the ERKtide substrate proved to be difficult due to its apparent high K_m value, which we predict is in the millimolar range. As a consequence, we were unable to determine solvent viscosity effects on k_{cat} for the phosphorylation of this substrate. To determine the $k_{cat}/K_{m(ERKtide)}$ value and the viscosity effect on this parameter, initial velocities at a single peptide concentration (50 μM) well below the predicted K_m value were determined as a function of increased sucrose concentration. The time course for phosphorylation in the absence of sucrose was linear, and doubling the substrate concentration both at zero viscosogen and at the highest relative viscosity resulted in a doubling of the initial rates, demonstrating that these rates, indeed, reflect true k_{cat}/K_m values.

The k_{cat}/K_m value for ERKtide was measured to be $(4 \pm 2) \times 10^{-3}$ μM^{-1} s^{-1}, and was unaffected by increasing solvent viscosity (Figure 5). This value is approximately 600-fold lower than that measured for MBP. The lack of a viscosity effect suggests that the dissociation rate constant for ERKtide is at least 10-fold greater than the maximal rate of phosphoryl group transfer. To place a lower limit on this value, we measured the rate of ERKtide phosphorylation at a single, high peptide substrate concentration (2 mM). The time course of phosphorylation was linear (not shown) and corresponded to an observed rate constant (k_{obs}) of 5.6 ± 0.4 s^{-1}. The maximal rate for the phosphoryl group transfer reaction therefore cannot be less than this value. As a consequence, a corresponding rate of 56 s^{-1} can be assigned as the lower limit rate of ERKtide dissociation from the active site, a value approximately 50-fold greater than the predicted maximal off-rate for MBP (Table 1). The available steady-state and viscosometric data for the phosphorylation of ERKtide are shown in Table 2.

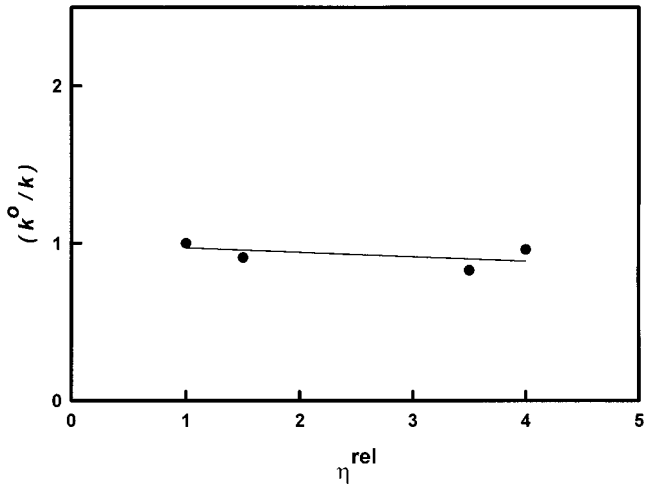

FIGURE 5: Solvent viscosity effects on k_{cat}/K_m for the phosphorylation of ERKtide. k^o/k corresponds to $(k_{cat}/K_{m(ERKtide)})^o/(k_{cat}/K_{m(ERKtide)})$. The superscript 'o' denotes the absence of viscosogen. η^{rel} is the relative solvent viscosity as defined under Materials and Methods. ATP was fixed at 1 mM; ERKtide was fixed at 50 and 100 μM. The viscosogenic agent was sucrose. The concentration of ERK2 was 50 nM.

DISCUSSION

The critical role that the MAP kinases play in signal transduction has placed this family of catalysts at the center of attention in terms of understanding their biochemical regulation and the physiological substrates that they target. In this study, we have characterized the catalytic reaction pathway of the dual-phosphorylated, fully active, mammalian ERK2 protein kinase with respect to the phosphorylation of both myelin basic protein (MBP) and a synthetic peptide substrate, ERKtide. Our studies lay the foundation on which the role of dual tyrosine and threonine phosphorylation in the activation process may ultimately be understood on a structure/mechanistic level. In addition, we describe the kinetic basis for high catalytic efficiency toward a protein substrate, MBP, as opposed to the best synthetic peptide substrate, ERKtide.

We determined the steady-state kinetic parameters for the phosphorylation of MBP by measuring initial reaction velocities at varied substrate concentration. A continuous assay was employed to monitor the true linear region of the reaction profile, which was observed to deviate from linearity early in the reaction time course at all MBP concentrations tested when ATP was fixed at 1 mM (Figure 1). The reaction profile was not changed upon doubling the concentration of coupling enzymes or by increasing the concentration of NADH by 10-fold. Furthermore, ERK2 proved to be stable over the entire reaction time course. The data could be fit to a Michaelis−Menten model which describes simple competitive product inhibition. Since product ADP is rapidly removed by the coupling system, we assume that the apparent product inhibition is due to the accumulation of phospho-MBP. However, we caution the interpretation of the K_p value ($\approx$0.5 μM) derived. While the phosphorylation of MBP by ERK2 has been mapped to a single site (Thr^{97}) at stoichiometries $\leq$0.4 mol of phosphate/mol of MBP (*20*), the amount of NAD^+ produced exceeded the initial concentration

Table 2: Kinetic and Thermodynamic Constants for Phosphorylation of ERKtide

parameter	value	method of determination
k_{cat}	$\geq 5.6\ s^{-1}$	measured at 2 mM ERKtide
$k_{cat}/K_{m(ERKtide)}$	$(4 \pm 2) \times 10^{-3}\ \mu M^{-1}\ s^{-1}$	$k_{cat}/K_{m(ERKtide)}$
k_{cat}^{η}	nd[a]	
$k_{cat}/K_{m(ERKtide)}^{\eta}$	-0.02 ± 0.02	measured
$k_{2(ERKtide)}$	$\geq 4 \times 10^{-2}\ \mu M^{-1}\ s^{-1}$	$(k_{cat}/K_{m(ERKtide)})/(k_{cat}/K_{m(ERKtide)}^{\eta})$
$k_{-2(ERKtide)}$	$\geq 56\ s^{-1}$	$k_3(1 - k_{cat}/K_{m(ERKtide)}^{\eta})/(k_{cat}/K_{m(ERKtide)}^{\eta})$
k_3	$\geq 5.6\ s^{-1}$	$k_{cat}/(1 - k_{cat}^{\eta})$
$K_{m(ERKtide)}$	$\geq 1500\ \mu M$	$k_{cat}/k_{cat}/K_{m(ERKtide)}$
$K_{d(ERKtide)}$	$\geq 1500\ \mu M$	$K_m/[k_4/(k_3 + k_4)]$[b]

[a] Not determined. [b] $k_4/(k_3 + k_4) \leq 1$.

of MBP by 2-fold (Figure 1), suggesting that when a large amount of the substrate is consumed multiple sites are phosphorylated. Furthermore, MBP purified from brain is heterogeneous, containing species which vary in their isoelectric points despite identical relative mobilities on SDS−PAGE (*34*). The derived inhibitory constant, therefore, is an apparent value owing to the intrinsic heterogeneity of the MBP and the phospho-MBP products formed. All steady-state parameters in this study, however, were determined from initial velocities, under which conditions the dependence of initial velocity vs MBP concentration obeyed classical Michaelis−Menten kinetics. While it has been reported that the phosphorylated, fully active form of ERK2 exists as a dimer in solution ($K_d = 7.5$ nM) (*35*), we have observed no evidence for kinetic interaction between the active sites within the dimer.

Steady-state kinetic analyses provide a lower limit value on the rates of substrate capture (k_{cat}/K_m) and release as product (k_{cat}), but provide little information on the individual reaction steps which constitute the complete catalytic reaction cycle. To access the microscopic rate constants of the partial reactions within the enzymatic mechanism of ERK2, we have perturbed the steady-state mechanism of MBP phosphorylation by altering the solvent viscosity using sucrose. The viscosity data are reported in Table 1. The observed viscosity effects on both k_{cat}/K_m and k_{cat} can be attributed specifically to the microviscosogenic properties of the cosolvent and not to the solvent macroviscosity, for the following reasons: (1) No viscosity effects on the kinetics of MBP phosphorylation were observed in the presence of a macroviscosogen, Ficoll 400. (2) No viscosity effects on the maximal ATPase rate for ERK2 were observed in the presence of sucrose. (3) No viscosity effects in sucrose were observed on k_{cat}/K_m for ERKtide, suggesting that the decrease in $k_{cat}/K_{m(MBP)}$ is not a result of substrate competition by sucrose.

We observed a partial viscosity effect on k_{cat} for the phosphorylation of MBP equal to 0.2, which is consistent with the overall rate of substrate processing being limited largely by the rate of the phosphotransfer step. Given a value of k_{cat} equal to 10 s^{-1}, it is predicted that the rate of phosphoryl group transfer is 12 s^{-1}. This value is nearly 50-fold lower than that for the phosphorylation of Kemptide by cAMP-dependent protein kinase (cAPK) (*36*), even though the catalytic efficiency of cAPK toward Kemptide (*25*) is equal to or lower than that of ERK2 toward MBP. Furthermore, in the case of cAPK, the release rate of product ADP is cleanly rate-limiting with respect to substrate processing (*25*), while the net rate of product release from ERK2 (56 s^{-1}) is rate-limiting to only a small extent.

Double-reciprocal plots obtained from nonlinear regression analysis using global fitting procedures (Figure 2) display a pattern of lines which intersect in the fourth quadrant, supporting a sequential mechanism. Furthermore, the crystal structure of the dual-phosphorylated ERK2 contains bound ATP in the absence of a protein substrate (*10*), and ERK2 displays measurable ATPase activity in the absence of MBP ($\sim$1 min^{-1} at 1 mM ATP; data not shown). Thus, our steady-state data are consistent with a kinetic mechanism which is either random or ordered with ATP binding first. Under saturating conditions of ATP, an ordered mechanism in which MBP binds to the free enzyme is not possible. $k_{cat}/K_{m(MBP)}$ therefore reports the addition of MBP to the E·ATP complex. The full viscosity effect observed on $k_{cat}/K_{m(MBP)}$ suggests that at low MBP concentrations, its rate of binding is limited by diffusion. In such a mechanism, formation of the Michaelis complex is followed by the immediate turnover of the bound substrates to form products. The release rate of substrate MBP from the active site is necessarily slower than the rate of phosphoryl group transfer by at least an order of magnitude. The derived rate value of 12 s^{-1} for phosphotransfer thus implies an upper limit rate of 1.2 s^{-1} for MBP dissociation. A consequence of the slow off-rate for MBP is that its K_d value is predicted to be at least 10-fold lower than the corresponding value for K_m (Table 1).

Results from viscosity experiments carried out at low ATP concentration at several fixed concentrations of MBP (Figure 4) suggest that the addition of substrates to ERK2 cannot be ordered. The full viscosity effect on $k_{cat}/K_{m(MBP)}$ (Figure 3) predicts that the net rate constant for the addition of MBP to the E·ATP complex [$k_2'[MBP] = k_2[MBP]k_3/(k_{-2} + k_3)$] reduces to $k_2[MBP]$. If an ordered mechanism (with ATP binding first) were assumed, the value for $k_{cat}/K_{m(ATP)}$ in such a mechanism would be given by $k_1k_2[MBP]/(k_{-1} + k_2[MBP])$, and the viscosity effect on this parameter [$k_{cat}/K_{m(ATP)}^{\eta} = k_2[MBP]/(k_{-1} + k_2[MBP])$] would be predicted to increase toward a maximum value of 1 as the concentration of MBP approached infinity. Our viscosity data display a clear *inverse* relationship between $k_{cat}/K_{m(ATP)}^{\eta}$ and MBP concentration (Figure 4) and, therefore, are inconsistent with an ordered binding mechanism. Rather, our data can be explained if the mechanism is assumed to be random. For example, we observe that the net rate constant for formation of the ternary E·ATP·MBP complex displays a full viscosity effect at low MBP, but no viscosity effect at high MBP (Figure 4). This is as expected if as the concentration of MBP approaches zero the ternary complex is formed predominantly by the addition of MBP to the E·ATP complex (Scheme 2). Under these conditions, this process is expected to be rate-limiting, and thus display a viscosity effect equal to 1. Similarly, as

the concentration of MBP approaches infinity, the ternary complex forms predominantly via the addition of ATP to the E·MBP complex; this process displays a viscosity effect equal to 0. The viscosity data (Figure 4) are consistent with the random addition of substrates in which the binding of MBP to the E·ATP complex is diffusion-limited, while the binding of ATP is in rapid exchange with the E·MBP complex.

The apparent second-order rate constant for the binding of MBP ($k_{cat}/K_m \approx 10^6$ M^{-1} s^{-1}) is among the highest reported for substrates of ERK2 (*21*) and of protein kinases, in general. The full viscosity effect observed on $k_{cat}/K_{m(MBP)}$ implies that the value for $k_{cat}/K_{m(MBP)}$ should correspond to the encounter frequency between MBP and the ERK2·ATP complex. While this is true, the predicted association rate constant ($k_{2(MBP)}$) lies 2−3 orders of magnitude below the theoretical upper limit for diffusion [10^8−10^9 M^{-1} s^{-1} (*37*)]. Two explanations can be offered. First, the upper limit on diffusion predicted by the Smoluchowski equation does not consider electrostatic effects on the frequency of encounter between two molecules (*37*). A calculated electrostatic surface potential of ERK2 reveals a high density of positive charge surrounding the active site (not shown). As MBP also displays a high overall net positive charge (pI > 12), electrostatic repulsion may be expected to significantly decrease the apparent encounter rate. Second, there is the possibility that multiple conformers of MBP and/or ERK2 may exist, among which only a small population of molecules may be productive, contributing to an apparent lower frequency of productive encounters (*38*).

The substrate determinants required by protein kinases for high catalytic efficiency have, in general, been largely unexplored on a structural level. In many cases, however, substrate specificity is determined almost entirely by the amino acid sequence surrounding the target phosphorylation site (*31, 39*). The key amino acid determinants for specific substrate recognition have classically been identified by systematic amino acid substitution analysis and recently by combinatorial peptide library screening (*40*). In these cases, short synthetic peptides containing the essential amino acid determinants serve as highly efficient substrates. The best example is cAPK, which recognizes the motif -R-R-X-S/T-Y- (Y = hydrophobic) and phosphorylates Kemptide (LRRASLG) with high catalytic efficiency (*31, 32*). Amino acid substitution analysis has defined the essential recognition motif for ERKs to be -X-P-X-S/T-P-X- (*7, 8, 41*), and a combinatorial library screen has identified ERKtide (ATGPLSPGPFGRR) as the optimal peptide substrate sequence (*33*). ERKtide, however, displays only poor catalytic efficiency toward ERK2. The k_{cat}/K_m value is 600-fold lower than that displayed by MBP.

We sought to investigate the mechanistic basis for the high catalytic efficiency of MBP ($k_{cat}/K_{m(MBP)}$) in comparison to that of ERKtide. A lack of a viscosity effect on the catalytic efficiency of ERKtide was observed, demonstrating that unlike the case with MBP, whose rate of binding is diffusion-limited, the binding of ERKtide is in rapid equilibrium with the enzyme active site. The dramatically lower catalytic efficiency of ERKtide compared to that of MBP is largely attributable to its greater rate of dissociation from ERK2. We found it unfeasible to conduct studies at saturating ERKtide concentrations due to its apparent high K_m value. We thus have been able to place only a lower limit value on the rate of phosphoryl group transfer ($\geq$5.6 s^{-1}) and, consequently, on the off-rate constant for ERKtide ($\geq$56 s^{-1}). This lower limit value ($k_{-2(ERKtide)}$) exceeds the maximum value for MBP ($k_{-2(MBP)}$) by approximately 50-fold. The true difference in the inherent dissociation rates of these two ligands may be greater.

While the k_{cat} value for ERKtide phosphorylation could not be definitively measured in this study, a rough approximation suggests that it is unlikely to differ from that of MBP by more that a few fold (not shown). The difference in catalytic efficiency between these two substrates, therefore, is not due to significant differences in the rates of their processing (k_{cat}). However, the difference in catalytic efficiency also cannot be directly correlated to differences in substrate binding affinity. The affinity of MBP for the ERK2·ATP ($K_{d(MBP)} \leq 0.5$ μM) complex is at least 3 orders of magnitude tighter than that calculated for ERKtide ($K_{d(ERKtide)} \geq 1500$ μM). While substrate affinity *is* a factor in determining the catalytic efficiency of ERKtide ($k_{cat}/K_{m(ERKtide)} \cong k_3/K_{d(ERKtide)}$), a thermodynamic expression for substrate binding is irrelevant when considering the catalytic efficiency of MBP which, in contrast, is controlled entirely by the kinetics of its diffusion to the ERK2 active site ($k_{cat}/K_{m(MBP)} \cong k_2$). For example, slowing of the dissociation rate constant for MBP, and therefore increasing its binding affinity, will not significantly increase the catalytic efficiency of this substrate. In contrast, small changes in the ERKtide dissociation rate constant (and therefore $K_{d(ERKtide)}$) will directly result in an equivalent alteration in ERKtide catalytic efficiency. The dramatically higher catalytic efficiency of MBP in comparison to ERKtide (~600-fold) is explained largely by the higher dissociation rates associated with the poorer synthetic peptide substrate.

In summary, the catalytic reaction pathway for ERK2 using a highly efficient substrate, MBP, consists of the diffusion-limited binding of MBP followed by phosphoryl group transfer which is slow in comparison to the release of products. This is in contrast to the kinetic mechanism established for the phosphorylation of Kemptide by cAPK ($k_{cat}/K_m \approx 0.3$ μM^{-1} s^{-1}), which comprises the rapid-equilibrium binding of the peptide substrate and the diffusion-limited binding of ATP, followed by fast chemical transfer and subsequent rate-limiting product release. The high catalytic efficiency of cAPK toward Kemptide is achieved by the high rate of chemistry associated with the cAPK·ATP·Kemptide complex [500 s^{-1} (*36*)] as opposed to that of the ERK2·ATP·MBP complex (12 s^{-1}). In contrast, the high catalytic efficiency of ERK2 toward MBP is attributable to the dramatically slower dissociation rate of MBP (<1.2 s^{-1}) from the ERK2 active site in comparison to the release rate of Kemptide (2000 s^{-1}) from the active site of cAPK (*25, 36*). At 10 mM free Mg^{2+}, the product release steps for both enzymes are of similar rates ($k_{4(ERK2)} = 56$ s^{-1}; $k_{4(cAPK)} = 20$ s^{-1}). While this process is limited by the release of ADP in the case of cAPK, our studies do not resolve the relative rates of release of the individual products from ERK2.

Peptides displaying high catalytic efficiency for protein kinases have historically been identified based on the corresponding amino acid sequence which surrounds the phosphorylation sites of known, highly efficient protein

substrates. In many cases, both the full-length protein and the corresponding synthetic peptide display comparable catalytic activity. For example, the k_{cat}/K_m values for a histone-derived peptide and histone protein toward cdk2/cyclin A are similar ($\sim$1 μM^{-1} s^{-1}, data not shown). A random peptide library screen has identified ERKtide as the optimal peptide substrate sequence for the ERKs (*33*). Although ERK1 was used in this screen, both ERK1 and ERK2 display nearly identical amino acid substrate sequence specificity (*8*). Given this fact, ERK2 displays 600-fold greater substrate specificity toward MBP than ERKtide, the latter which exhibits an approximate 3000-fold lower binding affinity with respect to forming the ternary Michaelis complex. The low apparent affinity is unlikely due to the possible increased conformational variability of the peptide versus the MBP protein, since these ligands are intrinsically distinct in terms of their binding kinetics, their dissociation rate constants ($k_{-2(ERKtide)}$ vs $k_{-2(MBP)}$) differing by a minimum of 50-fold, if not more. We speculate that the high stability of the ternary enzyme complex with respect to MBP binding is attributable to structural determinants which lie outside the minimal phosphorylation consensus sequence of this protein. Indeed, such substrate 'docking sites' have been identified in several other MAP kinase substrates, and have been shown to be critical for high catalytic efficiency (*42*). However, the reported sequences of these known docking site domains (*42*) are not conserved in MBP.

This study is the first to characterize the catalytic reaction pathway for the MAP kinase, ERK2, and is one of the few studies in which the kinetic parameters of a protein kinase toward a protein substrate have been determined. Using solvent viscosometric techniques, we have been able to assign rate constant values, or limits thereof, to each step in the overall kinetic mechanism for the phosphorylation of MBP. Our results provide a framework by which the structural and mechanistic basis for regulation by phosphorylation, substrate recognition, the role of active site residues, and potential inhibitor design may be understood.

ACKNOWLEDGMENT

We thank Drs. Stan Parsons and Joe Adams for extensive discussions, invaluable insight, and critical reading of the manuscript.

REFERENCES

1. Cobb, M. H. (1999) *Prog. Biophys. Mol. Biol. 71*, 479−500.
2. Cobb, M. H., and Goldsmith, E. J. (1995) *J. Biol. Chem. 270*, 14843−14846.
3. Lewis, T. S., Shapiro, P. S., and Ahn, N. G. (1998) *Adv. Cancer Res. 74*, 49−139.
4. Johnson, L. N., Noble, M. E., and Owen, D. J. (1996) *Cell 85*, 149−158.
5. Robinson, M. J., Cheng, M., Khokhlatchev, A., Ebert, D., Ahn, N., Guan, K. L., Stein, B., Goldsmith, E., and Cobb, M. H. (1996) *J. Biol. Chem. 271*, 29734−29739.
6. Ahn, N. G., Seger, R., and Krebs, E. G. (1992) *Curr. Opin. Cell Biol. 4*, 992−999.
7. Clark-Lewis, I., Sanghera, J. S., and Pelech, S. L. (1991) *J. Biol. Chem. 266*, 15180−15184.
8. Gonzalez, F. A., Raden, D. L., and Davis, R. J. (1991) *J. Biol. Chem. 266*, 22159−22163.
9. Shenoy, S., Choi, J. K., Bagrodia, S., Copeland, T. D., Maller, J. L., and Shalloway, D. (1989) *Cell 57*, 763−774.
10. Canagarajah, B. J., Khokhlatchev, A., Cobb, M. H., and Goldsmith, E. J. (1997) *Cell 90*, 859−869.
11. Zhang, F., Strand, A., Robbins, D., Cobb, M. H., and Goldsmith, E. J. (1994) *Nature 367*, 704−711.
12. Zhang, J., Zhang, F., Ebert, D., Cobb, M. H., and Goldsmith, E. J. (1995) *Structure 3*, 299−307.
13. Robinson, M. J., Harkins, P. C., Zhang, J., Baer, R., Haycock, J. W., Cobb, M. H., and Goldsmith, E. J. (1996) *Biochemistry 35*, 5641−5646.
14. Tonks, N. K., Diltz, C. D., and Fischer, E. H. (1988) *J. Biol. Chem. 263*, 6731−6737.
15. Gill, S. C., and von Hippel, P. H. (1989) *Anal. Biochem. 182*, 319−326.
16. Mansour, S. J., Candia, J. M., Matsuura, J. E., Manning, M. C., and Ahn, N. G. (1996) *Biochemistry 35*, 15529−15536.
17. Zhang, F., Robbins, D. J., Cobb, M. H., and Goldsmith, E. J. (1993) *J. Mol. Biol. 233*, 550−552.
18. Cook, P. F., Neville, M. E., Jr., Vrana, K. E., Hartl, F. T., and Roskoski, R. Jr. (1982) *Biochemistry 21*, 5794−5799.
19. Freifelder, D. (1982) *Physical Biochemistry: Applications to Biochemistry and Molecular Biology*, 2nd ed., W. H. Freeman and Co., New York.
20. Erickson, A. K., Payne, D. M., Martino, P. A., Rossomando, A. J., Shabanowitz, J., Weber, M. J., Hunt, D. F., and Sturgill, T. W. (1990) *J. Biol. Chem. 265*, 19728−19735.
21. Jacobs, D., Glossip, D., Xing, H., Muslin, A. J., and Kornfeld, K. (1999) *Genes Dev. 13*, 163−175.
22. Kramer, H. A. (1940) *Physica (Utrech) 7*, 284−304.
23. Blacklow, S. C., Raines, R. T., Lim, W. A., Zamore, P. D., and Knowles, J. R. (1988) *Biochemistry 27*, 683−733.
24. Brouwer, A. C., and Kirsch, J. F. (1982) *Biochemistry 21*, 1302−1307.
25. Adams, J. A., and Taylor, S. S. (1992) *Biochemistry 31*, 8516−8522.
26. Cole, P. A., Burn, P., Takacs, B., and Walsh, C. T. (1994) *J. Biol. Chem. 269*, 30880−30887.
27. Wang, C., Lee, T. R., Lawrence, D. S., and Adams, J. A. (1996) *Biochemistry 35*, 1533−1539.
28. Caldwell, S. R., Newcomb, J. R., Schlecht, K. A., and Raushel, F. M. (1991) *Biochemistry 30*, 7438−7444.
29. Nakatani, H., and Dunford, H. B. (1979) *J. Am. Chem. Soc. 83*, 2662−2665.
30. Phillips, H. O., Marcinkowsky, A. I., Sachs, S. B., and Kraus, K. A. (1977) *J. Phys. Chem. 81*, 679−682.
31. Kemp, B. E., and Pearson, R. B. (1990) *Trends Biochem. Sci. 15*, 342−346.
32. Kemp, B. E., Parker, M. W., Hu, S., Tiganis, T., and House, C. (1994) *Trends Biochem. Sci. 19*, 440−444.
33. Songyang, Z., Lu, K. P., Kwon, Y. T., Tsai, L. H., Filhol, O., Cochet, C., Brickey, D. A., Soderling, T. R., Bartleson, C., Graves, D. J., DeMaggio, A. J., Hoekstra, M. F., Blenis, J., Hunter, T., and Cantley, L. C. (1996) *Mol. Cell. Biol. 16*, 6486−6493.
34. Chou, F. C., Chou, C. H., Shapira, R., and Kibler, R. F. (1976) *J. Biol. Chem. 251*, 2671−2679.
35. Khokhlatchev, A. V., Canagarajah, B., Wilsbacher, J., Robinson, M., Atkinson, M., Goldsmith, E., and Cobb, M. H. (1998) *Cell 93*, 605−615.
36. Grant, B. D., and Adams, J. A. (1996) *Biochemistry 35*, 2022−2029.
37. Fersht, A. R. (1999) *Structure and Mechanism in Protein Science: A Guide to Enzyme Catalysis and Protein Folding*, W. H. Freeman and Co., New York.
38. Adams, J. A., and Taylor, S. S. (1993) *Protein Sci. 2*, 2177−2186.
39. Pinna, L. A., and Ruzzene, M. (1996) *Biochim. Biophys. Acta 1314*, 191−225.
40. Songyang, Z., Blechner, S., Hoagland, N., Hoekstra, M. F., Piwnica-Worms, H., and Cantley, L. C. (1994) *Curr. Biol. 4*, 973−982.
41. Alvarez, E., Northwood, I. C., Gonzalez, F. A., Latour, D. A., Seth, A., Abate, C., Curran, T., and Davis, R. J. (1991) *J. Biol. Chem. 266*, 15277−15285.
42. Holland, P. M., and Cooper, J. A. (1999) *Curr. Biol. 9*, R329−R331.

BI000277B